Classification of Colon Polyps in NBI Endoscopy Using Vascularization Features

Thomas Stehle and Roland Auer and Sebastian Gross and Alexander Behrens and Jonas Wulff and Til Aach and Ron Winograd and Christian Trautwein and Jens Tischendorf

Institute of Imaging and Computer Vision
RWTH Aachen University, 52056 Aachen, Germany
tel: +49 241 80 27860, fax: +49 241 80 22200
web: www.lfb.rwth-aachen.de

in: Medical Imaging 2009: Computer-Aided Diagnosis. See also BibTeX entry below.

Classification of Colon Polyps in NBI Endoscopy using Vascularization Features

Thomas Stehle[1], Roland Auer[1], Sebastian Gross[1,2], Alexander Behrens[1], Jonas Wulff[1],
Til Aach[1], Ron Winograd[2], Christian Trautwein[2] and Jens Tischendorf[2]

[1]Institute of Imaging & Computer Vision, RWTH Aachen University,
D-52056 Aachen, Germany

[2]Internal Medicine III, University Hospital Aachen, Pauwelsstr. 30,
D-52074 Aachen, Germany

ABSTRACT

The evolution of colon cancer starts with colon polyps. There are two different types of colon polyps, namely hyperplasias and adenomas. Hyperplasias are benign polyps which are known not to evolve into cancer and, therefore, do not need to be removed. By contrast, adenomas have a strong tendency to become malignant. Therefore, they have to be removed immediately via polypectomy. For this reason, a method to differentiate reliably adenomas from hyperplasias during a preventive medical endoscopy of the colon (colonoscopy) is highly desirable. A recent study has shown that it is possible to distinguish both types of polyps visually by means of their vascularization. Adenomas exhibit a large amount of blood vessel capillaries on their surface whereas hyperplasias show only few of them. In this paper, we show the feasibility of computer-based classification of colon polyps using vascularization features. The proposed classification algorithm consists of several steps: For the critical part of vessel segmentation, we implemented and compared two segmentation algorithms. After a skeletonization of the detected blood vessel candidates, we used the results as seed points for the Fast Marching algorithm which is used to segment the whole vessel lumen. Subsequently, features are computed from this segmentation which are then used to classify the polyps. In leave-one-out tests on our polyp database (56 polyps), we achieve a correct classification rate of approximately 90%.

Keywords: Polyp, classification, colon, cancer, endoscopy, colonoscopy, vessel segmentation

1. INTRODUCTION

Cancer of the colon is the fourth most common type of cancer and the second leading cause of cancer death in the USA. The greatest risk factors are age, and personal and family history of cancer.[1] But other factors like a chronic inflammatory bowel disease,[2] smoking, physical inactivity, alcohol, and diabetes[3] increase the risk of developing colorectal cancer as well. Each year more than 135,000 new cases are diagnosed and over 56,000 people die from colorectal cancer in the United States.

The evolution of colon cancer starts with colon polyps. There are two different types of colon polyps, namely hyperplasias and adenomas. Hyperplasias are benign polyps which are known not to evolve into cancer. In contrast, adenomas have a strong tendency to develop cancer (via the so called adenoma-carcinoma sequence[4]) and, therefore, they have to be removed immediately via a polypectomy. Hyperplasias which do not hamper the normal colon function should not be removed as every polypectomy poses a risk for the patient (in about 10% of all cases a polypectomy causes a complication[5]). Indeed, polypectomies can cause serious bleedings in

---

the patient's colon if the patient is on blood thinning pharmaceuticals. They may even cause perforations of the colon.

In 1994 Kudo et al. published a method[6] to distinguish visually between adenomas and hyperplasias. It is based on the so called pit pattern which describes a polyp's surface structure. Pit patterns can only be observed during chromo endoscopy where a dye is sprayed onto the polyp. If the pit pattern shows roundish spots, the polyp is likely to be hyperplastic. If the pit pattern shows tubular or villous structures, the polyp it is likely to be adenomatous. After the polyp inspection, the staining must be flushed away as it hampers the detection of further polyps. Possibly, the endoscope's lens becomes stained as well and needs to be cleaned before the polyp can be inspected.

A recent study[7] has shown that the classification of colon polyps by means of vascularization features provides a sensitivity and specificity which are comparable to those of Kudo's method. For the detection of vessels on colon polyps, an imaging technology to enhance vessels like narrow band imaging (NBI) must be applied. In NBI, a special light source is used in front of which a color filter wheel rotates. In this filter wheel, several optical narrow band pass filters are integrated which produce an illumination well absorbed by hemoglobin. Therefore, blood vessels can be distinguished more reliably from the remaining polyp tissue compared to normal white light endoscopy. This technology is much easier to use than chromo endoscopy as the physician can switch the light source from white light mode to NBI mode and back at any time.

We propose an algorithm consisting of several stages, which are reflected by the structure of our paper. In the following section, we describe the preprocessing in which differences in illumination are reduced and specular reflections detected on the polyp's surface are excluded from further processing. In sec. 3, we elaborate on the evaluated vessel segmentation algorithms. In sec. 4 we derive vascularization features which were selected in cooperation with two specialists in endoscopic colon examination. Subsequently, we give information on our polyp database, explain the classifier we use, and show the results. In sec. 5, we conclude the paper with a summary of our method.

2. PREPROCESSING

Images acquired during an endoscopy of the colon exhibit properties which hamper their analysis. As the colon's surface is wet and the light source is parallel to the optical axis, it is very likely that specular reflections occur on the polyp surfaces. These specular reflections need to be detected and excluded from later analysis. A further problem is the inhomogeneous illumination. The endoscope's light source is focused on the center of the field of view which leads to strong vignetting. Furthermore, the distance from the endoscope to the polyp differs from image to image so the overall illumination strength varies between images. In this section, we describe how to detect specular reflections and compensate for inhomogeneous illumination.

2.1 Detection of Specular Reflections

Several algorithms for detection of specular reflections are known in literature. Gevers[8] proposed the comparison of two different color spaces to detect them. His basic idea is to use one color space in which edges caused by texture changes as well as edges from specular reflections are observable. The other color space is only sensitive to edges caused by texture changes and therefore the difference of both edge images contains the edges of the specular reflections.

We found, however, that detection of specular reflections can be accomplished faster and easier exploiting the fact that specular reflections exhibit very low color saturations. Unfortunately, not only very bright pixels but also very dark pixels exhibit low saturations. To avoid the detection of these pixels as specular reflections we perform an additional test on the pixel's brightness value. The test to identify specular reflections can by summarized by

$$\text{isSpecularReflection} = \left\{ \begin{array}{ll} \text{true,} & \text{if } (\text{Saturation} < t_1) \,\&\, (\text{Value} > t_2) \\ \text{false,} & \text{otherwise} \end{array} \right. \tag{1}$$

where Saturation and Value are the respective components of the HSV color space, and t_1 and t_2 are the thresholds on saturation and value, respectively. As this kind of segmentation usually tends to a slight under-segmentation, a morphological dilatation is used to enlarge the segmented areas using a disc-shaped structure element. Fig. 1 shows an example of specular reflections successfully detected by the described method.
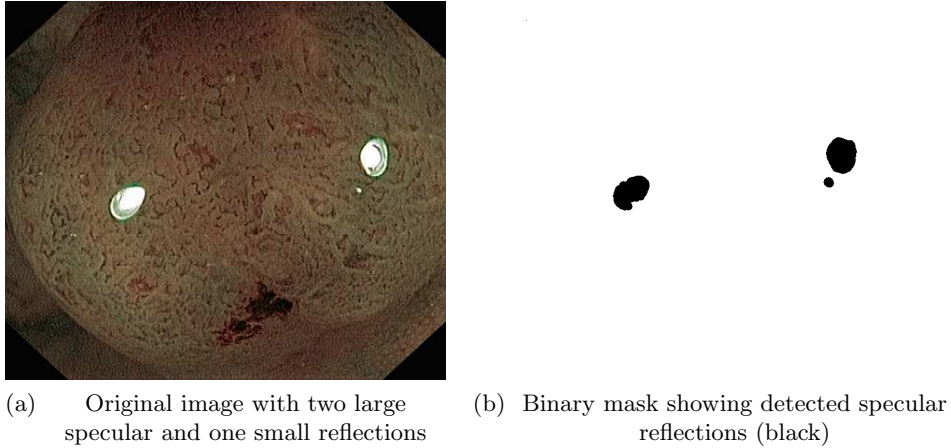
(a)   Original image with two large   (b)   Binary mask showing detected specular
specular and one small reflections   reflections (black)

Figure 1. Detection of specular reflections

2.2 Gray Value Conversion and Normalization of Image Brightness

From now on, we restrict our algorithm to work on monochromatic images. Therefore, like in ophthalmology, we use the green color channel as it provides the best contrast for blood vessels.[9] To reduce the effect of inhomogeneous illumination, we now normalize the image brightness locally to the interval [0, 1]. To this end, each pixel's value is divided by the maximum value of the pixel's local neighborhood, e. g. a 13×13 neighborhood.

3. VESSEL SEGMENTATION

As vessel segmentation is a critical part of our algorithm, we tested and compared two different algorithms: A combination of Bredno's directional stamping algorithm[10] and Frangi's vesselness filter,[11] and a combination of Kovesi's features from phase symmetry[12] and Sethian's fast marching.[13] In the following, these algorithms are shortly summarized.

3.1 Directional Vesselness Stamping

The directional stamping algorithm relies on the structure tensor[14] to identify oriented image content. The structure tensor

$$T = \int_\Omega \begin{pmatrix} g_x g_x & g_x g_y \\ g_x g_y & g_y g_y \end{pmatrix} d\Omega \tag{2}$$

contains information on the orientation of the local gray level structure. Ω is the local neighborhood of the pixel to be analyzed, and g_x and g_y are the partial derivatives of the gray value image g in x and y direction, respectively. These derivatives are computed by convolutions with derivatives of a Gaussian function, i. e.

$$g_x = g * \frac{\partial}{\partial x} \left(\frac{1}{2\pi \sqrt{|\Sigma|}} \exp\left(-\frac{1}{2} \vec{x}^T \Sigma^{-1} \vec{x} \right) \right) \tag{3}$$

where $\vec{x} = (x, y)^T$, Σ is the covariance matrix, $|.|$ is the determinant and $*$ is the convolution operator. The derivatives in y direction are computed analogously.

For analysis, the structure tensor's eigenvalues λ_1 and λ_2 (without loss of generality $\lambda_1 \geq \lambda_2$) with the respective eigenvectors $\vec{\nu}_1$ and $\vec{\nu}_2$ are considered. In the case of two large eigenvalues, more than one orientation is present in the area Ω and the orientations cannot be determined using the structure tensor. If one eigenvalue is large and the other one is small, one oriented structure (possibly a blood a vessel) is present in the image and it is aligned with $\vec{\nu}_2$. The angle δ of the orientation can be computed by

$$\delta = atan2(\nu_{2,y}, \nu_{2,x}) \tag{4}$$

where $\nu_{2,y}$ and $\nu_{2,x}$ are the y and x components of the vector $\vec{\nu_2}$, respectively, and $atan2$ is the quadrant-aware arcus-tangens function.

If both eigenvalues are small, no considerable structure is present in the current area Ω. As the structure tensor is positive semi-definite, only zero-valued or positive eigenvalues can occur and, therefore, the sign of the eigenvalue cannot be used to distinguish bright from dark structures.

For each detected oriented pixel, the values of an elliptically shaped Gaussian function

$$G(\vec{x}) = \frac{1}{2\pi\sqrt{|L|}} \exp\left(-\frac{1}{2}\vec{x}^T L^{-1}\vec{x}\right) \tag{5}$$

with the covariance matrix

$$L = \begin{pmatrix} \cos(\delta) & -\sin(\delta) \\ \sin(\delta) & \cos(\delta) \end{pmatrix} \begin{pmatrix} \lambda_1 & 0 \\ 0 & \lambda_2 \end{pmatrix} \begin{pmatrix} \cos(\delta) & -\sin(\delta) \\ \sin(\delta) & \cos(\delta) \end{pmatrix}^T \tag{6}$$

is calculated. This Gaussian is rotated and scaled in a manner such that it locally approximates the blood vessel. Subsequently, it is multiplied with the texture patch around the detected oriented pixel and then forms the so called stamp

$$S^* = G \cdot g \tag{7}$$

For each oriented pixel, the stamp is generated and added to or (metaphorically speaking) stamped onto an accumulator image, which was initialized with zeros. After all pixels are processed, the accumulator exhibits high values at locations where oriented structures (possibly blood vessels) occur.

Because the directional stamping algorithm as described above was too sensitive, we combined it with the vesselness filter to achieve more reliable results. The vesselness filter relies on the second order derivatives of a gray value image. The second order derivatives are computed by successive convolutions with Gaussian derivatives as shown in Eq. (3).

Therewith, the Hessian matrix

$$H = \begin{pmatrix} g_{xx} & g_{xy} \\ g_{xy} & g_{yy} \end{pmatrix} \tag{8}$$

can be computed where the g_{xx}, g_{xy} and g_{yy} are the second order derivatives. The eigenvalues γ_1 and γ_2 (without loss of generality $|\gamma_1| \geq |\gamma_2|$, here $|.|$ is the absolute value) of the Hessian give information on the locally present gray value variation. Two eigenvalues with large absolute values indicate a disc-shaped gray value structure. If one eigenvalue's absolute value is large and the other one is small or equal to zero, an elongated structure like a blood vessel is the locally predominant structure. If both eigenvalues are (small or) equal to zero the gray values in the examined area are (nearly or) totally constant. Therefore, the expression

$$V_1 = \left(1 - \exp\left(-\left|\frac{\gamma_1}{\gamma_2 \cdot \alpha}\right|\right)\right) \tag{9}$$

is close to one if an elongated structure is present at the current image location. Here, α is a regulation parameter. For robustness against noise, only strong gray value variations should be detected. A measure for the strength of the gray level variation is the Frobenius norm $||.||_F$ of the Hessian matrix, which can be expressed elegantly using both its eigenvalues

$$||H||_F^2 = \gamma_1^2 + \gamma_2^2. \tag{10}$$

Therefore, the expression

$$V_2 = \left(1 - \exp\left(-\frac{\gamma_1^2 + \gamma_2^2}{\beta}\right)\right) \tag{11}$$

is close to one in the case of strong gray level variations and close to zero otherwise. β is another fine tuning parameter.
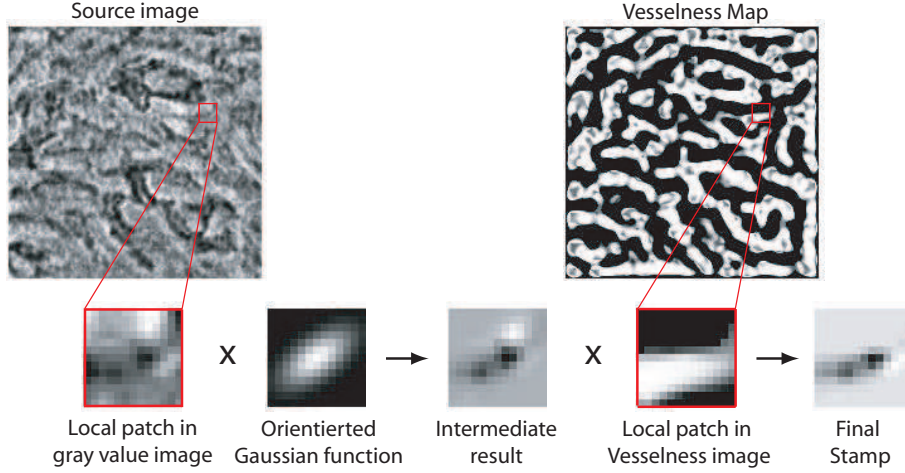
Figure 2. Directional Vesselness Stamping

The sign of γ_1 gives information on whether there is a dark structure on bright background or vice versa. In our case, the blood vessels are dark on bright background and, therefore, only locations where $\gamma_1 > 0$ are of interest. So finally, the vesselness can be expressed as

$$V = \begin{cases} 0, & \text{if } \gamma_1 \leq 0 \\ V_1 \cdot V_2, & \text{otherwise} \end{cases} \tag{12}$$

and the combined directional vesselness stamp is defined as the directional stamp from Eq. (7) additionally weighted with the vesselness V, such that it reads

$$S = G \cdot V \cdot g \tag{13}$$

Fig. 2 shows an example of a gray level image and the corresponding vesselness image. Additionally, it depicts the process of the directional vesselness stamp generation. Fig. 3 shows the segmentation results for an adenoma (left column) and a hyperplasia (right column).

3.2 Phase Symmetry

The phase symmetry measure is based on a local spatial frequency and phase analysis of the image. The fact that symmetric structures exhibit a characteristic distribution of phase information is then exploited to identify blood vessel candidates.

In Fig. 4 the main idea of phase symmetry is depicted. At the top, an example of a gray level profile through a blood vessel is shown and at the bottom there is its Fourier decomposition. One can observe that the symmetry axis of the profile is also the symmetry axis of the Fourier decomposition. Moreover, all base functions exhibit local extrema, i. e. they are all even-symmetric functions with a phase difference of 180 degrees. This feature of phase symmetry (dominance of even-symmetric Fourier components) characterizes symmetric structures like blood vessels.

In the following, only a short summary of the computation of phase symmetry is given. For a comprehensive presentation of phase symmetry, Kovesi's papers[12, 15] are highly recommended.

The local phase analysis is carried out using a set of quadrature wavelet pairs. Here, *Log Gabor* wavelets are used. If the even and odd symmetric wavelets at scale n are denoted by M_n^e and M_n^o, respectively, the filter response vector can be expressed as
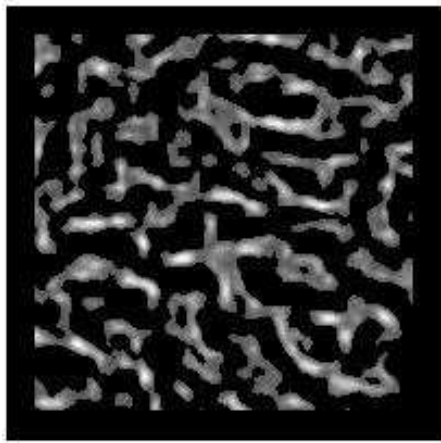
$$\begin{pmatrix} e_n(\vec{x}) \\ o_n(\vec{x}) \end{pmatrix} = \begin{pmatrix} g(\vec{x}) * M_n^e \\ g(\vec{x}) * M_n^o \end{pmatrix} \tag{14}$$
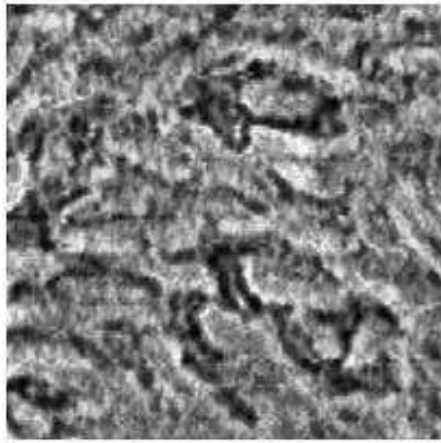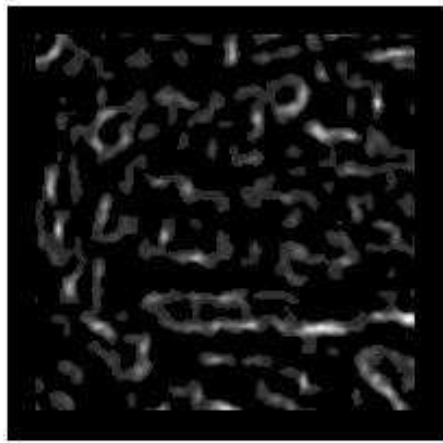
(a) Source image (adenoma)
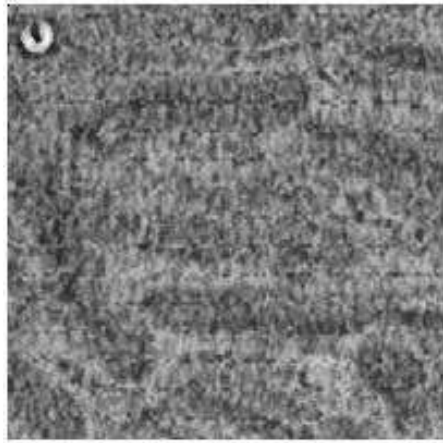
(b) Source image (hyperplasia)

(c) Directional vesselness stamping

(d) Directional vesselness stamping

(e) Result

(f) Result

Figure 3. Example of vessel detection using directional vesselness stamping. Left column: adenoma. Right column: hyperplasia.
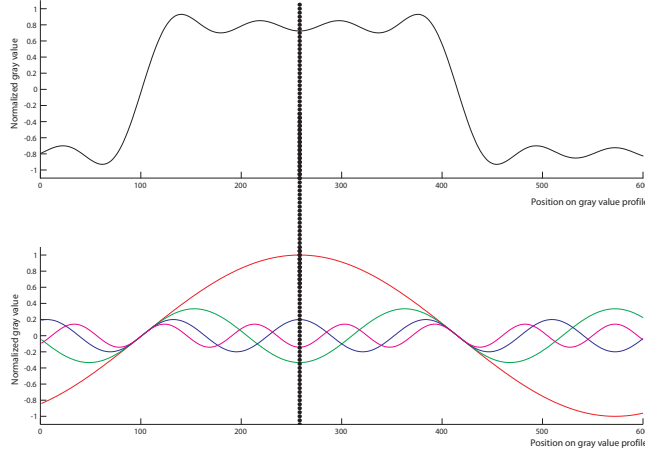
Figure 4. Top: Example of a gray value profile through a blood vessel. Bottom: Fourier analysis of the blood vessel profile. One can observe that the phase difference of the different base function in the middle of the blood vessel is 180 degrees. The symmetry axis of the vessel is also the symmetry axis for all Fourier components.

where e_n and o_n are the even and odd filter responses at scale n, respectively. The corresponding amplitude is given by

$$A_n(\vec{x}) = \sqrt{e_n(\vec{x})^2 + o_n(\vec{x})^2} \tag{15}$$

and the phase is given by

$$\Phi_n(\vec{x}) = atan2(e_n(\vec{x}), o_n(\vec{x})) \tag{16}$$

The phase symmetry can now be computed by

$$sym(\vec{x}) = \frac{\sum_n \lfloor |e_n(\vec{x})| - |o_n(\vec{x})| - T \rfloor}{\sum_n A_n(\vec{x}) + \epsilon}. \tag{17}$$

As stated earlier, the dominance of even-symmetric components characterizes symmetric structures. In Eq. (17), the absolute values of the even-symmetric components are summed up, whereas the absolute values of the odd-symmetric components are subtracted. Therefore, the numerator is large if the even-symmetric components outweigh the odd-symmetric ones. The parameter T is a threshold which accounts for image noise and the operator $\lfloor . \rfloor$ is defined as

$$\lfloor x \rfloor = \begin{cases} x, & \text{if } x > 0 \\ 0, & \text{otherwise} \end{cases} \tag{18}$$

The denominator in Eq. (17) normalizes to the sum of all spectral amplitudes and the term ϵ prevents divisions by zero.

The results of the phase symmetry measure can be seen in Figs. 5(c) and 5(d) for an adenoma and a hyperplasia, respectively. As evidently not the whole vessel lumen is segmented, it is necessary to take further steps to achieve this goal. To this end, the results were first skeletonized[16, 17] and these pixel locations were handed to a region growing algorithm as seed points. As region growing algorithm we chose Sethian's fast marching algorithm.[13, 18] Since the region is expanded in directions which cause the lowest cost, a cost function has to be defined and handed over to the fast marching algorithm. As cost function we chose

$$cost(\vec{x}) = s(g(\vec{x})) - \varphi \cdot sym(\vec{x}). \tag{19}$$

where s is a sigmoidal function for enhancement of contrast between vessels and background and φ is a weighting factor. With this cost function, the cost in dark blood vessels is lower than in the bright surroundings. The cost in blood vessels is further reduced by the subtraction of the weighted phase symmetry measure. The results of this step can be seen in the last row of Fig. 5.
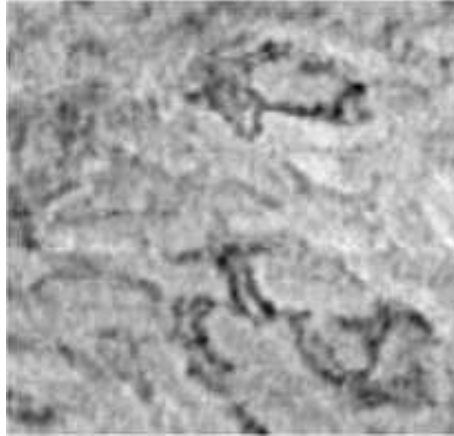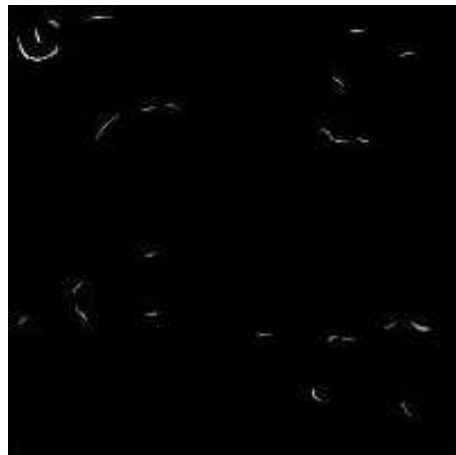
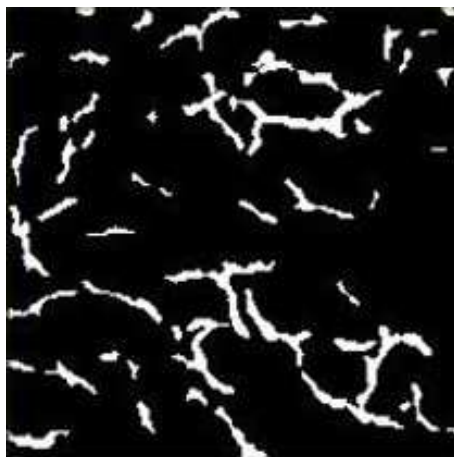(a) Source image (adenoma)
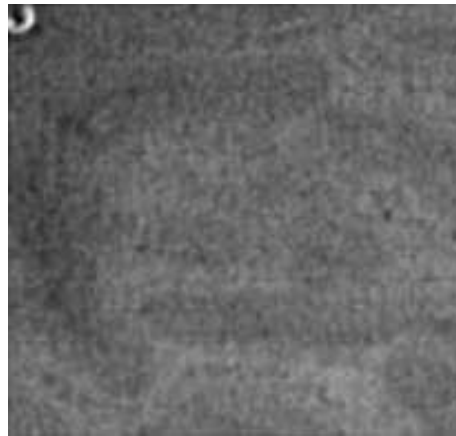
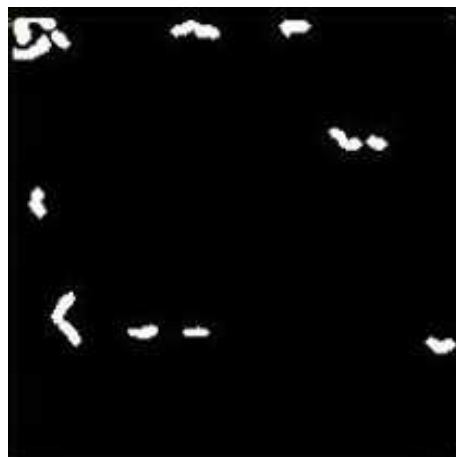(b) Source image (hyperplasia)
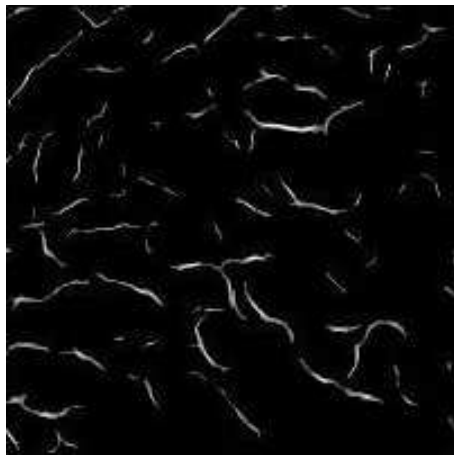
(c) Result phase symmetry

(d) Result phase symmetry

(e) Result fast marching

(f) Result fast marching

Figure 5. Example of vessel segmentation using phase symmetry. Left column: adenoma. Right column: hyperplasia.

3.3 Experiments and Results

As determining whether or not a pixel belongs to a blood vessel is very difficult even for an experienced physician, we decided to use a gold standard that allows a range of possible correct segmentations. Fig. 6(a) shows a section of an adenoma surface. In Figs. 6(b) and 6(c) two different gold standard segmentations are shown, which were carried out by our research group's specialists in endoscopic colon examination. In Fig. 6(b) all pixels were marked which definitely belong to blood vessels whereas in Fig. 6(c) all pixels were marked which most probably belong to blood vessels. In the evaluation of the segmentation, the result is regarded as correct if at least all pixels from the gold standard with low sensitivity (Fig. 6(b)) but not more pixels than the pixels in the gold standard with high sensitivity (Fig. 6(c)) are segmented. In Figs. 6(f), 6(g) and 6(h) the original image, the gold standard segmentation with low sensitivity and the gold standard segmentation with high sensitivity are shown for a hyperplasia, respectively.
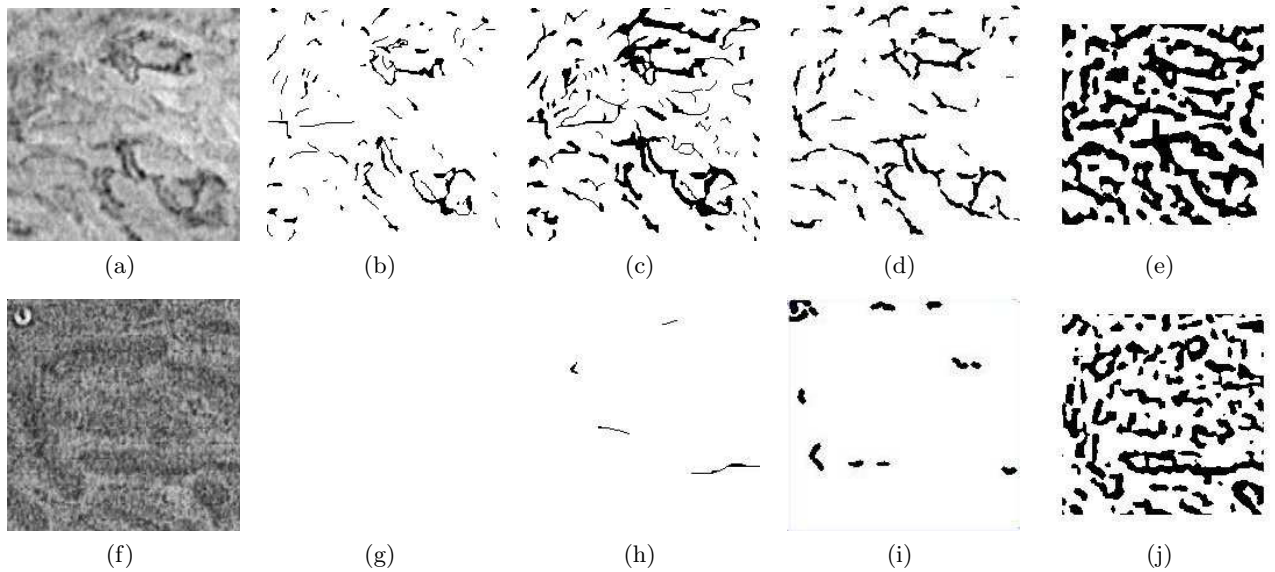

| (a) | (b) | (c) | (d) | (e) |
| (f) | (g) | (h) | (i) | (j) |

Figure 6. Top row: (a) green color channel of an adenoma's surface, (b) gold standard segmentation with low sensitivity, (c) gold standard segmentation with high sensitivity, (d) result of automatic segmentation using phase symmetry and fast marching, (e) result of automatic segmentation using directional vesselness stamping. Bottom row: respective images of a hyperplasia.

Figs. 6(d) and 6(i) show exemplary results of the combination of the phase symmetry filter and the fast marching algorithm whereas Figs. 6(e) and 6(j) show the result of directional vesselness stamping. Evidently, the directional vesselness stamping is still too sensitive for a reliable blood vessel detection.

Table 1. Results of automatic vessel segmentation using directional vesselness stamping and phase symmetry combined with fast marching. The phase symmetry based algorithm clearly delivers superior results.

	Directional vesselness stamping		Phase symmetry + fast marching	
	Adenoma	Hyperplasia	Adenoma	Hyperplasia
#vessel pixels	5287	151	5287	151
#non-vessel pixels	30901	32761	30901	32761
#false positives	7447	9696	587	833
#false negatives	175	0	402	0
#true negatives	20027	22914	26887	31777
#true positives	1685	0	1458	0
absolute error	7662	9696	989	833
relative error	**35.1%**	**42.3%**	**3.5%**	**2.6%**

For a quantitative analysis of the segmentation results, five polyps were segmented manually by the experts and, subsequently, the algorithms were applied to these images. Tab. 1 summarizes the results of this experiment. The relative errors of directional vesselness stamping were 35.1% and 45.3% for the adenomas and hyperplasias, respectively. The errors for the combination of phase symmetry and fast marching, however, were only 3.5% and 2.6% for adenomas and hyperplasias, respectively. For this reason, the combination of phase symmetry and fast marching was used in the following for vessel segmentation.

4. CLASSIFICATION AND RESULTS

For the classification of polyps, discriminative features for classification had to be chosen. To this end, two specialists in endoscopic colon examination in our research group defined a set of features which was then evaluated. The feature set contained the features which the physicians regarded as most important. These were vessel length, area, and contrast. Further features were circumference, branching factor and the mean brightness value at detected vessel positions.

Our dataset consisted of 56 polyps (37 adenomas and 19 hyperplasias). Each polyp was imaged using NBI and removed from the patient's colon. Then, the polyp tissue was analyzed histologically such that a reliable ground truth was available.

In our first classification experiment, three features (mean gray value at detected vessel locations, vessel length and mean vessel circumference) were chosen together with a linear classifier - namely a decision plane in the three dimensional feature space. The plane's normal was defined to point along the connection line between the adenoma and hyperplasia cluster centers. The plane's position was varied until the best possible result was reached. As only very limited data was available, we decided to carry out leave-one-out tests. That means the decision plane was defined using 55 polyps and the remaining one was then classified. With this setup we achieved a correct classification rate of 89.2%. This corresponds to a sensitivity of 91.9% and a specificity of 84.2%.

In a second experiment, we defined the optimal decision plane manually to evaluate how good both classes can be separated under optimal conditions. In this case, a correct classification rate of 94.6% could be achieved which corresponds to a sensitivity of 100% and a specificity of again 84.2%.

A visualization of the feature space with the optimal decision plane is presented in Fig. 7. The polyps marked with boxes are misclassified as being adenomas. The removal of these polyps might unnecessarily cause complications like bleedings or performation. In these cases, however, the consequences for the patients are less critical than in case of wronlgy classifying an adenoma as being a hyperplasia. In this case, the patient would run the risk of developing cancer.
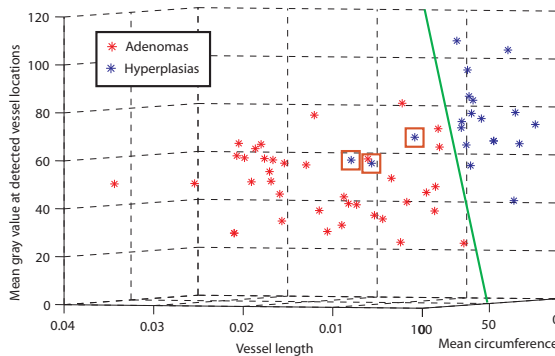

Figure 7. Visualization of the three dimensional feature space with an optimal decision plane. Using the mean gray value at detected vessel locations, the vessel length and the mean circumference as features, a classification rate of approximately 94% can be achieved using a linear classifier.

5. SUMMARY AND CONCLUSION

We have described a multi-stage system for the automatic feature extraction and classification of colon polyps. During preprocessing of the analyzed image data, specular reflections were detected and excluded from later analysis. Furthermore, as illumination in endoscopic images can heavily change, a normalization of image brightness was subsequently carried out.

Vessel segmentation was a critical component and, therefore, two different vessel segmentation algorithms - the directional vesselness stamping and a combination of phase symmetry and fast marching - were implemented and evaluated. During the evaluation, we found that the combination of phase symmetry and fast marching gave the best results.

Segmentations achieved with this combination were used to compute several vascularization features. The most promising ones (vessel length, mean gray level at vessel centerlines and mean vessel circumference) were used in leave-one-out classification experiments. On our polyp database (56 polyps with histological ground truth), we achieved a correct classification rate of approximately 90%, which corresponds to a sensitivity of 91.9% and a specificity of 84.2%.

REFERENCES

[1] Fuchs, C. S., Giovannucci, E. L., Colditz, G. A., Hunter, D. J., Speizer, F. E., and Willett, W. C., "A prospective study of family history and the risk of colorectal cancer.," *N Engl J Med* **331**, 1669–1674 (Dec 1994).

[2] Bernstein, C. N., Blanchard, J. F., Kliewer, E., and Wajda, A., "Cancer risk in patients with inflammatory bowel disease," *Cancer* **91**(4), 854–862 (2001).

[3] Marchand, L. L., Wilkens, L. R., Kolonel, L. N., Hankin, J. H., and Lyu, L.-C., "Associations of Sedentary Lifestyle, Obesity, Smoking, Alcohol Use, and Diabetes with the Risk of Colorectal Cancer," *Cancer Res* **57**(21), 4787–4794 (1997).

[4] Gloor, F. J., "The adenoma-carcinoma sequence of the colon and rectum," *Social and Preventive Medicine* **31**, 74–75 (March 1986).

[5] Heldwein, W., Dollhopf, M., Rsch, T., Meining, A., Schmidtsdorff, G., Hasford, J., Hermanek, P., Burlefinger, R., Birkner, B., Schmitt, W., and Group, M. G., "The Munich Polypectomy Study (MUPS): prospective analysis of complications and risk factors in 4000 colonic snare polypectomies.," *Endoscopy* **37**, 1116–1122 (Nov 2005).

[6] Kudo, S., Hirota, S., Nakajima, T., Hosobe, S., Kusaka, H., Kobayashi, T., Himori, M., and Yagyuu, A., "Colorectal tumours and pit pattern.," *J Clin Pathol* **47**, 880–885 (Oct 1994).

[7] Tischendorf, J. J. W., Wasmuth, H. E., Koch, A., Hecker, H., Trautwein, C., and Winograd, R., "Value of magnifying chromoendoscopy and narrow band imaging (NBI) in classifying colorectal polyps: a prospective controlled study.," *Endoscopy* **39**(12), 1092–1096 (2007).

[8] Gevers, T., "Reflectance-based classification of color edges," *Proceedings of the Ninth IEEE International Conference on Computer Vision* , 856–861 (Oct. 2003).

[9] Hajer, J., Kamel, H., and Noureddine, E., "Blood vessels segmentation in retina image using mathematical morphology and the stft analysis," in [*Information and Communication Technologies, 2006. ICTTA '06. 2nd*], **1**, 1130–1134 (24-28 April 2006).

[10] Bredno, J., Martin-Leung, B., and Eck, K., "Algorithmic solutions for live device-to-vessel match," *SPIE Medical Imaging: Image Processing* (2004).

[11] Frangi, A. F., Niessen, W. J., Vincken, K. L., and Viergever, M. A., "Multiscale vessel enhancement filtering," *Lecture Notes in Computer Science* **1496**, 130–137 (1998).

[12] Kovesi, P., "Image features from phase congruency," *Videre Journal of Research* **1**(3), 2–26 (1999).

[13] Sethian, J., "A fast marching level set method for monotonically advancing fronts," *Proceedings of the National Academy of Science* **93**, 1591–1595 (1996).

[14] Bigün, J. and Granlund, G. H., "Optimal orientation detection of linear symmetry," *Proceedings of the IEEE First International Conference on Computer Vision* , 433–438 (June 1987).

[15] Kovesi, P., "Symmetry and asymmetry from local phase," in [*Tenth Australian Joint Conference on Artificial Intelligence*], 185–190 (December 1997).

[16] Guo, Z. and Hall, R. W., "Parallel thinning with two-subiteration algorithms," *Comm. ACM* **32**(3), 359–373 (1989).

[17] Zhang, T. Y. and Suen, C. Y., "A fast parallel algorithm for thinning digital patterns," *Comm. ACM* **84**(3), 236–239 (1984).

[18] Deschamps, T., *Curve and Shape Extraction with Minimal Path and Level-Sets Technique-Applications to 3D Medical Imaging*, PhD thesis, Universit Paris-IX Dauphine (2001).